LETTERS

Chemical reduction of three-dimensional silica micro-assemblies into microporous silicon replicas

Zhihao Bao[1], Michael R. Weatherspoon[1], Samuel Shian[1], Ye Cai[1], Phillip D. Graham[1], Shawn M. Allan[1], Gul Ahmad[1], Matthew B. Dickerson[1], Benjamin C. Church[1], Zhitao Kang[1], Harry W. Abernathy III[1], Christopher J. Summers[1], Meilin Liu[1] & Kenneth H. Sandhage[1]

The carbothermal reduction of silica into silicon requires the use of temperatures well above the silicon melting point (≥2,000 °C)[1]. Solid silicon has recently been generated directly from silica at much lower temperatures (≤850 °C) via electrochemical reduction in molten salts[2,3]. However, the silicon products of such electrochemical reduction did not retain the microscale morphology of the starting silica reactants[2,3]. Here we demonstrate a low-temperature (650 °C) magnesiothermic reduction process for converting three-dimensional nanostructured silica micro-assemblies into microporous nanocrystalline silicon replicas. The intricate nanostructured silica microshells (frustules) of diatoms (unicellular algae) were converted into co-continuous, nanocrystalline mixtures of silicon and magnesia by reaction with magnesium gas. Selective magnesia dissolution then yielded an interconnected network of silicon nanocrystals that retained the starting three-dimensional frustule morphology. The silicon replicas possessed a high specific surface area (>500 $m^2 g^{-1}$), and contained a significant population of micropores (≤20 Å). The silicon replicas were photoluminescent, and exhibited rapid changes in impedance upon exposure to gaseous nitric oxide (suggesting a possible application in microscale gas sensing). This process enables the syntheses of microporous nanocrystalline silicon micro-assemblies with multifarious three-dimensional shapes inherited from biological[4–6] or synthetic silica templates[7–9] for sensor, electronic, optical or biomedical applications[10–13].

Silica diatom frustules were converted into MgO/Si-bearing replicas by the following reaction with gaseous Mg:

$$2Mg(g) + SiO_2(s) \rightarrow 2MgO(s) + Si(s) \quad (1)$$

Images of a silica *Aulacoseira* diatom frustule, and of a reacted MgO/Si-bearing product, are shown in Fig. 1a and b, respectively. *Aulacoseira* frustules have a hollow cylindrical shape. Their end faces contain a circular hole with a protruding outer rim. These frustules were lined with rows of fine pores (10^2 nm in diameter) running along the cylinder length, and also contained narrow channels between intercalating fingerlike extensions. The MgO/Si composites (Fig. 1b) generated by reaction (1) retained the three-dimensional (3D) cylindrical morphology and nanoscale features (rows of fine pores, narrow channels) of the *Aulacoseira* frustules. X-ray diffraction (XRD) analysis (Fig. 2a) confirmed the presence of magnesia and silicon in the reacted specimens. The MgO/Si composite replicas were then immersed in a 1 M HCl solution for 4 h. XRD (Fig. 2b) and energy dispersive X-ray (Fig. 1e) analyses indicated that this treatment resulted in the selective and complete dissolution of magnesia.

The resulting silicon-based product (Fig. 1c) retained the 3D morphology and nanoscale features of the *Aulacoseira* frustules (see Supplementary Fig. 1 for images of other diatom frustule replicas). The energy dispersive X-ray pattern in Fig. 1e contained a modest oxygen peak, which was associated with amorphous silica (silicon dioxide) formed during exposure of the silicon to the water-rich HCl solution. The replicas were then immersed in an ethanol-based hydrofluoric acid (HF) solution for 20 min. The absence of an oxygen peak in the energy dispersive X-ray pattern in Fig. 1f indicated that the silica had been completely and selectively dissolved by this HF

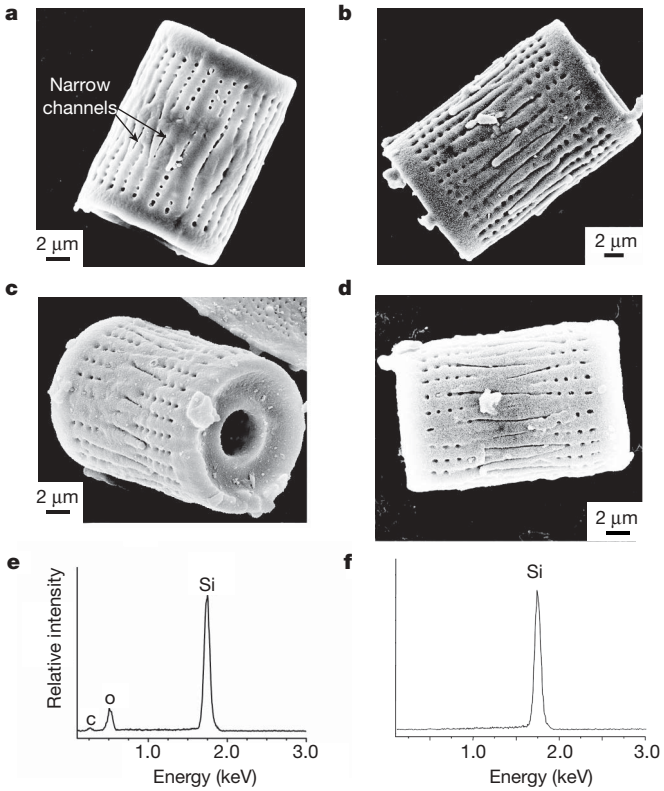

Figure 1 | Shape-preserving magnesiothermic reduction of silica diatom frustules. a, Secondary electron image of an *Aulacoseira* diatom frustule. **b**, Secondary electron image of a MgO/Si composite replica after reaction of an *Aulacoseira* frustule with Mg(g) at 650 °C for 2.5 h. **c**, Secondary electron image of a silicon-bearing replica produced by selective dissolution of magnesia from a MgO/Si replica in an HCl solution. **d**, Secondary electron image of a silicon replica after the HCl treatment and an additional treatment in a HF solution. **e**, **f**, Energy dispersive X-ray analyses obtained from silicon frustule replicas of the type shown in **c** and **d**, respectively.

[1]School of Materials Science & Engineering, Georgia Institute of Technology, Atlanta, Georgia 30332, USA.

treatment. X-ray photoelectron spectroscopy (Supplementary Fig. 2) and Fourier transform infrared spectroscopy (Supplementary Fig. 3) also confirmed the absence of silica in the specimens after the HF treatment. The replicas exposed to this HF treatment (Fig. 1d) retained the shape and fine features of the starting frustules.

A mixture of one mole of silicon with two moles of magnesia (the products of reaction (1)) corresponds to 34.9 vol.% silicon and 65.1 vol.% magnesia[14]. A uniform distribution of silicon and magnesia in such a product mixture should consist of co-continuous, interpenetrating silicon and magnesia phases[15]. The interconnectivity of both phases enabled the magnesia to be completely dissolved from the MgO/Si frustule replicas and the remaining silicon to be retained as a highly porous, but interconnected structure that preserved the starting frustule morphology. Nitrogen adsorption (Brunauer–Emmett–Teller, BET) measurements indicated that the specific surface areas of the starting silica frustules and of the MgO/Si composite replicas were only 1.65 $m^2 g^{-1}$, and 1.56 $m^2 g^{-1}$, respectively. After magnesia removal, however, the specific surface area increased to 541 $m^2 g^{-1}$. BJH (Barrett–Joyner–Halenda) analyses[16] of the nitrogen desorption curves indicated that, unlike the starting frustules or MgO/Si replicas, the silicon replicas possessed a significant population of micropores; that is, pores $\leq$2 nm in diameter comprised 30% of the cumulative volume occupied by all pores $\leq$125 nm in diameter (Supplementary Fig. 4).

The use of magnesium gas as a reducing agent enabled the reduction process to be conducted at a modest temperature, at which the formation of volatile silicon-bearing gas species (such as SiO(g), Si(g)) was suppressed[17]. As a result, the reduction reaction could be completed on and within the frustules (and not within the gas phase away from the frustule surfaces) to yield MgO/Si-bearing replicas. This modest 650 °C/2.5 h heat treatment, along with the formation of a continuous refractory magnesia phase intertwined with the silicon product, inhibited substantial coarsening and sintering of the silicon product, so that features as fine as a few tens of nanometres in the starting silica diatom frustules could be preserved in the silicon replicas after selective magnesia dissolution (see Supplementary Fig. 1). Although a few authors have previously examined the reaction of silica with magnesium gas, the shape preservation and microporosity of the liberated (magnesia-free) silicon product generated by such reaction were not examined[18–20].

Transmission electron images of cross-sections of a silicon frustule replica are shown in Fig. 3a–d. A corresponding selected area electron diffraction pattern is shown in Fig. 3e. Consistent with XRD analysis (Fig. 2b), electron diffraction analysis indicated the presence of silicon as the only crystalline phase throughout the replica cross-section. The fine sizes of the silicon crystals (Fig. 3b) detected within the wall of the converted frustule were also consistent with Scherrer analysis[21] of the XRD pattern in Fig. 2b, which yielded an average silicon crystallite size of 13 $\pm$ 2 nm. The high-resolution transmission electron image shown in Fig. 3c and the associated Fourier-filtered version of this image in Fig. 3d both reveal lattice fringe images of adjacent silicon nanocrystals. The continuation of the lattice fringe patterns from these adjacent grains up to the grain boundary indicated that this grain boundary was free of an amorphous silica phase. Grain boundaries between other adjacent silicon nanocrystals were also found to be free of an amorphous phase. Some of the silicon crystals located at the outer surfaces of the silicon replicas were relatively large (~30 nm; Fig. 3b). A modified protocol was used to reduce further the average size of the crystals in the silicon replicas. The MgO/Si composite replicas were immersed in an aqueous solution of 1.1 M hydrogen peroxide and 2.2 M ammonium hydroxide at 70 °C for 0.5 h partially to oxidize the silicon grains (particularly the relatively coarse grains on the external replica surfaces). The specimens were then immersed in HF and HCl solutions to selectively dissolve the silica and magnesia, respectively. Scherrer analysis of the XRD pattern obtained from such silicon replicas yielded a reduced average silicon crystallite size of 8 $\pm$ 1 nm.

Planar (two-dimensional) microporous silicon has been used as a sensor for various gas species[11,22–24]. The high specific surface areas and open (accessible) structures of the present 3D silicon frustule replicas are attractive characteristics for use in sensitive and rapid gas detection. To evaluate such gas detection, a simple sensor based on a silicon frustule replica was fabricated (Fig. 4a). Platinum electrodes were used to connect the ends of this replica to gold pads (not shown) deposited on a silicon nitride substrate. A modest bias voltage (100 mV at 100 Hz) was applied across the electroded silicon frustule

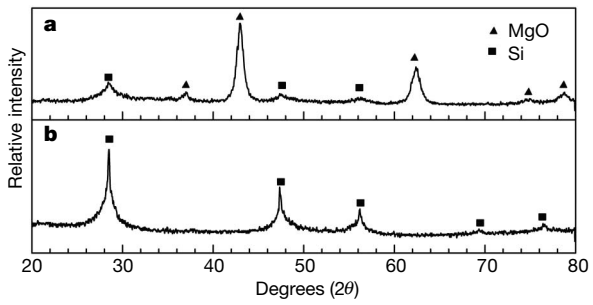

Figure 2 | Phase content of diatom frustules after magnesiothermic reduction. **a**, XRD pattern revealing the presence of magnesia and silicon formed after exposure of *Aulacoseira* silica diatom frustules to magnesium gas at 650 °C for 2.5 h. **b**, XRD pattern obtained after selective dissolution of the magnesia from the MgO/Si composites in **a**.

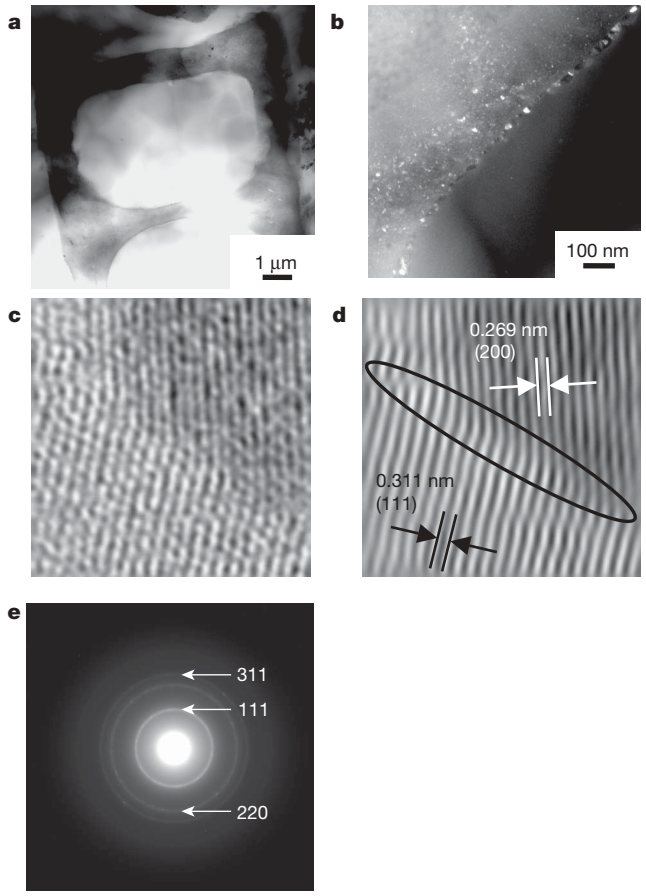

Figure 3 | Fine-scale structure of silicon replicas produced by magnesiothermic reduction of *Aulacoseira* diatom frustules. **a**, **b**, Low-magnification bright field and higher-magnification dark field transmission electron images, respectively, of an ion-milled cross-section of a silicon frustule replica. **c**, High-resolution transmission electron image of adjacent silicon nanocrystallites. **d**, The same image in **c** after Fourier filtering. **e**, Selected area electron pattern obtained from the silicon frustule replica shown in **a** and **b**.

replica, and the change in impedance was evaluated upon exposure to flowing NO(g) in an Ar(g) carrier stream at 300 °C. The impedance of the silicon frustule sensor increased upon exposure to low (p.p.m.) concentrations of NO(g) (Fig. 4b). Furthermore, changes of only 1 p.p.m. in NO(g) concentration could be detected. The response (rise) and recovery (decay) times of this sensor were about 6 and 25 s, respectively, which are faster times than has been reported for planar porous silicon sensors exposed to comparable NO(g) concentrations[23]. Such a combination of rapid (≤25 s) and sensitive (1 p.p.m.) detection of NO(g) from a microscale (minimally invasive) 3D silicon sensor operating with a bias voltage of only 100 mV (instead of several volts) has not previously been achieved, to our knowledge. Although further work remains to be conducted to optimize the packaging of such a sensor, the high sensitivity and rapid response rate of the silicon frustule replica demonstrate the benefits of such an open, porous, 3D structure with such high surface area.

Several authors have also reported the photoluminescence of microporous silicon in ultraviolet light, particularly after partial oxidation in water[25,26]. To evaluate such photoluminescence, the silicon frustule replicas were partially oxidized by immersion in water for 40 days. The photoluminescence of the 3D silicon frustule replicas was dramatically enhanced after such partial oxidation (Supplementary Fig. 5a and b). A fluorescence microscope image of such a photoluminescent silicon frustule replica is shown in Supplementary Fig. 5c.

The present work demonstrates that microporous assemblies of silicon nanocrystals with intricate and well-controlled 3D morphologies may be synthesized by the shape-preserving magnesiothermic reduction of microscale silica-based structures at only 650 °C. Biologically replicable silica-forming microorganisms, such as diatoms, can provide a wide variety of intricate 3D silica structures for this reduction process[4]. Sustained culturing of a given diatom species can yield significant quantities of 3D silica frustules of similar morphology. For example, the diatom biomass production rate of a single pilot-scale facility with 45 vertical bubble column photobioreactors can be in excess of 700 kg (dry weight) per annum[27], which corresponds to an annual silica frustule yield in excess of 70 kg (assuming a modest 10 wt% silica content in the dry cells[28]). The magnesiothermic reduction process is also amenable to scale-up (the current yield of the authors' laboratory-scale magnesiothermic reduction process is 100 mg h^{-1}, which is comparable to the 20–200 mg h^{-1} production rate of silicon nanoparticles via laser-induced pyrolysis of silane[29]). Hence, by applying the shape-preserving magnesiothermic reduction process to biologically or synthetically self-assembled silica templates, large quantities of similar 3D silicon nanocrystal assemblies with precisely controlled microscale shapes and nanoscale features (pores, channels and so on) may be synthesized for use in sensor, electronic, optical, biochemical, or other applications[10–13].

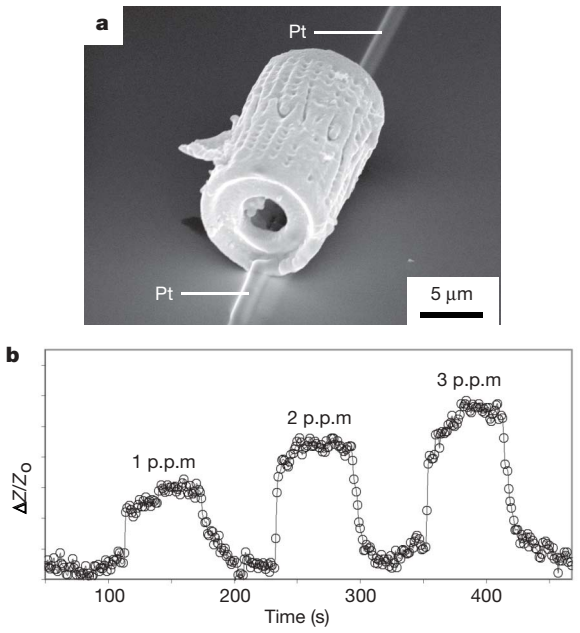

Figure 4 | Gas sensor based on a silicon frustule replica. a, Secondary electron image of an electroded microporous silicon frustule replica. **b**, Electrical response of this single silicon frustule sensor to NO(g). ΔZ is the impedance change upon exposure to NO(g), and Z_o is the sensor impedance in pure flowing argon. Measurements were obtained every second.

METHODS

Conversion of silica diatom frustules into microporous silicon replicas. Diatom frustules were spread evenly within a steel boat to form a 0.2-mm-deep powder bed. The frustule-bearing steel boat and magnesium granules were placed at opposite ends of a steel ampoule that was then welded shut. The $Mg:SiO_2$ molar ratio sealed within each ampoule was 2.5:1. Such ampoules were thrust into a tube furnace that had been preheated to 650 °C, and then held at this temperature for 2.5 h (at 650 °C, the oxygen and nitrogen partial pressures associated with the Mg/MgO and Mg/Mg_3N_4 equilibria are only 1.7×10^{-57} atm and 3.1×10^{-16} atm, respectively[17]). The reacted frustules were observed to contain three regions of different colour. The region located nearest the magnesium gas source was blue in colour. A black region and then a brown region were observed with increasing distance from the magnesium gas source. XRD analyses indicated that each region contained magnesia (magnesium oxide). The black and brown regions also contained silicon as a secondary product phase, whereas the blue region contained magnesium silicide, Mg_2Si (which is a blue-coloured intermetallic compound[14]). Residual, unreacted silica (in the form of cristobalite) was detected in the brown region. The MgO/Si composite material located in the black region of the reacted frustule bed was collected and immersed in a 1 M HCl solution (molar $HCl:H_2O:EtOH$ ratio = 0.66:4.72:8.88) for 4 h at room temperature to selectively dissolve the magnesia. The specimens were then exposed to a HF solution (molar $HF:H_2O:EtOH$ ratio = 1.05:1.11:6.45) to ensure that any silica formed during exposure to the aqueous HCl treatment was removed. The HCl treatment and the subsequent HF treatment were conducted within an argon atmosphere glove box. The argon in this glove box was obtained from an ultrahigh-purity tank (99.999% purity) and this gas was further scrubbed of oxygen with an oxygen gettering system. The oxygen partial pressure in this glove box was maintained at below 0.1 p.p.m. (as determined by an oxygen sensor).

Characterization of the microporous silicon replicas. The infrared spectra for FTIR measurements were recorded using a Bruker Equinox 55 spectrometer with a liquid N_2-cooled MCT detector. Measurements were made in diffuse reflectance mode using a Praying Mantis DRIFTS attachment from Harrick Scientific. Both the spectrometer and DRIFTS attachment were continuously purged with N_2 gas to minimize the background signal from atmospheric CO_2 and H_2O. The spectra obtained were averages of 128 scans recorded at 4 cm^{-1} resolution. The sample spectra, measured from samples consisting of ~10 vol.% silicon frustule replicas mixed with KBr powder, were referenced to a background of pure KBr powder. XPS analyses were conducted with a Kratos Axis-165 instrument (Kratos Analytical, Manchester, UK) using monochromatic Al Kα radiation. The specimens were transferred into the XPS instrument under an argon atmosphere. After removal from the HF-bearing solution, the specimens were allowed to dry in the argon atmosphere glove box. The frustule replicas were pressed onto 0.25-mm-thick indium foil and then sealed in plastic bags within the glove box. The sealed bags were then placed inside a glove bag that was, in turn, sealed around the evacuable antechamber of the XPS. After the glove bag was purged with ultrahigh-purity (99.999%) argon, the specimens were removed from the plastic bags and placed inside the antechamber. The antechamber was then evacuated for XPS analyses. Milling of the specimens within the XPS system was conducted with Ar^+ ions. XPS analyses were calibrated with respect to the carbon 1*s* excitation (285.0 eV).

For gas-sensing measurements, a single silicon frustule (*Aulacoseira*) replica was placed on a silicon nitride substrate and platinum electrodes were then applied to both ends of the replica with the aid of a focused ion beam instrument. A potentiostat was used to impose a small bias voltage (100 mV at 100 Hz) across the silicon frustule sensor, and to monitor the corresponding current passing through the sensor, during switching of the sample gas from pure argon to argon containing different concentrations of NO(g) at 300 °C.

The photoluminescence spectrum was obtained with a Spex 1000M spectrometer using an argon laser, with an emission wavelength of 275 nm (ultraviolet) and a power of 5 mW, as the excitation source. The laser was focused to a spot of ~1 mm in diameter on the sample. The photoluminescence measurements were

performed at room temperature and recorded with a GaAs photomultiplier tube with a cutoff wavelength of 920 nm. Fluorescence microscopy was conducted using a Zeiss Axiovert 200 microscope, with a fluorescence excitation of 450–490 nm.

Scanning electron microscopy was conducted with a Leo/Zeiss 1530 field emission scanning electron microscope operating at an accelerating voltage of 10 kV. Transmission electron microscopy was conducted with a JEOL 4000 EX microscope operating at an accelerating voltage of 400 kV.

Received 13 November 2006; accepted 2 January 2007.

1. Nagamori, M., Malinsky, I. & Claveau, A. Thermodynamics of the silicon-carbon-oxygen system for the production of silicon carbide and metallic silicon. *Metall. Trans. B* **17,** 503–514 (1986).
2. Nohira, T., Yasuda, K. & Ito, Y. Pinpoint and bulk electrochemical reduction of insulating silicon dioxide to silicon. *Nature Mater.* **2,** 397–401 (2003).
3. Yasuda, K., Nohira, T., Takahashi, K., Hagiwara, R. & Ogata, Y. H. Electrolytic reduction of a powder-molded SiO_2 pellet in molten $CaCl_2$ and acceleration of reduction by Si addition to the pellet. *J. Electrochem. Soc.* **152,** D232–D237 (2005).
4. Round, F. E., Crawford, R. M. & Mann, D. G. *The Diatoms: Biology and Morphology of the Genera* (Cambridge Univ. Press, New York, 2000).
5. Aizenberg, J. *et al.* Skeleton of Euplectella sp.: structural hierarchy from the nanoscale to the macroscale. *Science* **309,** 275–278 (2005).
6. Hall, S. R., Bolger, H. & Mann, S. Morphosynthesis of complex inorganic forms using pollen grain templates. *Chem. Commun.* 2784–2785 (2003).
7. Blaaderen, A., Ruel, R. & Wiltzius, P. Template-directed colloidal crystallization. *Nature* **385,** 321–324 (1997).
8. Cha, J. N., Stucky, G. D., Morse, D. E. & Deming, T. J. Biomimetic synthesis of ordered silica structures mediated by block copolypeptides. *Nature* **403,** 289–292 (2000).
9. Fan, H. *et al.* Rapid prototyping of patterned functional nanostructures. *Nature* **405,** 56–60 (2000).
10. Cullis, A. G. & Canham, L. T. Visible light emission due to quantum size effects in highly porous crystalline silicon. *Nature* **353,** 335–338 (1991).
11. Baratto, C. *et al.* Front-side micromachined porous silicon nitrogen dioxide gas sensor. *Thin Solid Films* **391,** 261–264 (2001).
12. Shin, H.-C., Corno, J. A., Gole, J. L. & Liu, M. Porous silicon negative electrodes for rechargeable lithium batteries. *J. Power Sources* **139,** 314–320 (2005).
13. Bengtsson, M. *et al.* Applications of microstructured porous silicon as a biocatalytic surface. *Phys. Status Solidi A* **182,** 495–504 (2000).
14. *Powder Diffraction File* Card No. 27–1402 for Si, Card No. 45–946 for MgO, Card No. 35–0773 for Mg_2Si (International Center on Diffraction Data, Newtown Square, Pennsylvania); ⟨www.icdd.com⟩.
15. Bouvard, D. & Lange, F. F. Relation between percolation and particle coordination in binary powder mixtures. *Acta Metall. Mater.* **39,** 3083–3090 (1991).
16. Barrett, E. P., Joyner, L. G. & Halenda, P. P. The determination of pore volume and area distributions in porous substances. I. Computations from nitrogen isotherms. *J. Am. Chem. Soc.* **73,** 373–380 (1951).
17. Barin, I. *Thermochemical Data of Pure Substances* 3rd edn, pages 994, 1012, 1014, 1481, 1504, 1505 (VCH, Weinheim, 1995).
18. Wynnyckyj, J. R. & Rao, D. B. The mechanism of reduction of silica by magnesium vapor. *High Temp. Sci.* **8,** 203–217 (1976).
19. Banerjee, H. D., Sen, S. & Acharya, H. N. Investigations on the production of silicon from rice husks by the magnesium method. *Mater. Sci. Eng.* **52,** 173–179 (1982).
20. Sandhage, K. H. *et al.* Novel, bioclastic route to self-assembled, 3D, chemically tailored meso/nanostructures: shape-preserving reactive conversion of biosilica (diatom) microshells. *Adv. Mater.* **14,** 429–433 (2002).
21. Cullity, B. D. *Elements of X-ray Diffraction* 101–102 (Addison-Wesley, Reading, Massachusetts, 1978).
22. Watanabe, K., Okada, T., Choe, I. & Sato, Y. Organic vapor sensitivity in a porous silicon device. *Sensors Actuators B* **33,** 194–197 (1996).
23. Boarino, L. *et al.* NO_2 monitoring at room temperature by a porous silicon gas sensor. *Mater. Sci. Eng. B* **69–70,** 210–214 (2000).
24. Seals, L., Gole, J. L., Tse, L. A. & Hesketh, P. J. Rapid, reversible, sensitive porous silicon gas sensor. *J. Appl. Phys.* **91,** 2519–2523 (2002).
25. Balagurov, L. A., Leiferov, B. M., Petrova, E. A., Orlov, A. F. & Panasenko, E. M. Influence of water and alcohols on photoluminescence of porous silicon. *J. Appl. Phys.* **79,** 7143–7147 (1996).
26. Gelloz, B., Kojima, A. & Koshida, N. Highly efficient and stable luminescence of nanocrystalline porous silicon treated by high-pressure water vapour annealing. *Appl. Phys. Lett.* **87,** 031107 (2005).
27. Miron, A. S., Gomez, A. C., Camacho, F. G., Grima, E. M. & Chisti, Y. Comparative evaluation of compact photobioreactors for large-scale monoculture of microalgae. *J. Biotechnol.* **70,** 249–270 (1999).
28. Schmid, A.-M. M., Borowitzka, M. A. & Volcani, B. E. in *Cytomorphogenesis in Plants* (ed. Kiermayer, O.) Cell Biology Monographs 8 63–97 (Springer, Vienna, 1981).
29. Li, X., He, Y., Talukdar, S. S. & Swihart, M. T. Process for preparing macroscopic quantities of brightly photoluminescent silicon nanoparticles with emission spanning the visible spectrum. *Langmuir* **19,** 8490–8496 (2003).

Supplementary Information is linked to the online version of the paper at www.nature.com/nature.

Acknowledgements This work was supported by the US Air Force Office of Scientific Research (H. C. DeLong and J. Fuller) and the US Office of Naval Research (M. Spector). We thank M. Bestor for assistance with XPS analysis and S. Yoo for help with focused ion beam milling.

Author Contributions Z.B., M.R.W., S.M.A., P.D.G., M.B.D. and K.H.S. conceived, developed and demonstrated the low-temperature magnesiothermic reduction and selective dissolution process. S.S. prepared and tested silicon replica gas sensors. G.A. cultured diatoms for conversion. Transmission electron microscope and BET analyses were conducted by Y.C. and B.C.C., respectively. H.W.A. and M.L. conducted and analysed FTIR measurements. Z.K. and C.J.S. conducted and analysed photoluminescence measurements. M.B.D. conducted fluorescence microscopy. Overall data analyses, project planning and paper preparation were largely conducted by Z.B. and K.H.S.

Author Information Reprints and permissions information is available at www.nature.com/reprints. The authors declare no competing financial interests. Correspondence and requests for materials should be addressed to K.H.S. (ken.sandhage@mse.gatech.edu).